

Improved efficiency of dye-sensitized solar cells by design of a proper double layer photoanode electrodes composed of Cr-doped TiO₂ transparent and light scattering layers

M. R. Mohammadi · A. M. Bakhshayesh ·
F. Sadri · M. Masroor

Received: 20 January 2013 / Accepted: 23 April 2013 / Published online: 30 April 2013
© Springer Science+Business Media New York 2013

Abstract A new strategy for enhancing the efficiency of TiO₂ dye-sensitized solar cells (DSSCs) by design of a new double layer film doped with Cr ions, with various morphologies, is reported. X-ray diffraction and field emission scanning electron microscope (FE-SEM) analyses revealed that the synthesized nanoparticles had uniform and nanometer grains with different phase compositions and average crystallite size in the range of 10–12 nm depending upon Cr atomic percentage. UV–vis absorption showed that Cr introduction enhanced the visible light absorption of TiO₂ nanoparticles by shifting the absorption onset to visible light region. Furthermore, the band gap energy of nanoparticles decreased with an increase in dopant concentration due to reduction of particle size. It was found that, 3 at.% Cr-doped TiO₂ DSSC in the form of a double-layer film composed of TiO₂ nanoparticles, as the under-layer, and mixtures of nano- and micro-particles with weight ratio of 80:20, as the over-layer, (i.e., CT3/NM3 solar cell) had the highest power conversion efficiency of 7.02 %, short current density of 17.32 mA/cm² and open circuit voltage of 674 mV. This can be related to achievement of a balance among the electron injection, light scattering effect and dye sensitization parameters. Optimization of light scattering effect of photoanode electrode led to improve the photovoltaic performance of CT3/NM3 double-layer solar cell and was demonstrated by diffuse reflectance spectroscopy. The presented strategy would open up new insight into fabrication of low-cost TiO₂ DSSCs with high power conversion efficiency.

Keywords Cr-doped TiO₂ · Dye-sensitized solar cell · Light scattering effect · Double layer film

1 Introduction

In the present age, dye-sensitized solar cells (DSSCs) have been regarded as a promising candidate for third solar cells generation owing to their ease of manufacturing, good power conversion efficiency and low cost [1]. This class of cell has reached efficiencies over 12 % recently [2]. When sunlight radiates onto the DSSC the electrons in the highest occupied molecular orbital of the dye absorb photons that become excited and jump to the lowest unoccupied molecular orbital (LUMO). The electrons from the LUMO level are then injected into the anatase-TiO₂ semiconductor conduction band and pass through the TiO₂ layer to the transparent conductive oxide coated glass and to a load [3]. In order to reach high conversion efficiencies, it is important to increase the electron injection and optical absorption. One promising solution to increase the electron injection is to decrease the large band gap of TiO₂ by doping a foreign ion into TiO₂ lattice [4]. A wide range of metal ions such as iron [5], nickel [6], copper [7], manganese [8] and cobalt [9] have been used as acceptor dopants into TiO₂. In addition, niobium as a donor dopant has been used for fabrication of TiO₂ solar cell [10]. The result showed that the conversion efficiency of a cell based on 5.0 mol% Nb-doped TiO₂ was about 18.2 % higher than that of a cell based on undoped TiO₂. Several studies have been reported on the effect of Cr introduction, as a dopant, on optical and photocatalyst properties of TiO₂ [11–13]. Since Cr³⁺ has a lower number of valence electrons than Ti⁴⁺, the excess holes can create an acceptor band near TiO₂ valence band. Because of the lower band gap between

M. R. Mohammadi (✉) · A. M. Bakhshayesh · F. Sadri ·
M. Masroor
Department of Materials Science and Engineering, Sharif
University of Technology, Azadi Street, Tehran, Iran
e-mail: mrm41@cam.ac.uk; mohammadi@sharif.edu

the valance and acceptor, the migration of electrons from valance to acceptor band could be take place in a lower temperature. Peng et al. [14] investigated the effects of Cr-doping concentration and annealing temperature on the photocatalytic activity of TiO₂. The results show that, the absorption edges of TiO₂ thin films shift effectively from 375 nm to about 800 nm with increasing Cr concentration. Choudhury and Choudhury [11] studied the optical properties of Cr-doped TiO₂ thin film prepared by sol–gel method and found that incorporation of Cr produces a progressive shift of the absorption threshold toward the visible. Lyson et al. [15] synthesized Cr-doped TiO₂ nanoparticles with dopant concentration from 0.1 to 10 at.% by a liquid-fed one-step flame spray synthesis. They showed that the band gap is shifted from about 3.0 eV for undoped TiO₂ to about 1.5 eV for 10 at.% Cr-doped TiO₂. Recently, Xie et al. [16] fabricated double layer dye-sensitized solar cells based on Cr-doped TiO₂ films and found that the DSSC made of 50 ppm dopant had higher photovoltaic performance (e.g., power conversion efficiency of 6.35 %) than the DSSC made of undoped nanoparticles (power conversion efficiency of 5.54 %). The light scattering is already a well-known approach for boosting the optical absorption of photoelectrode in the conventional DSSCs [17] and can be realized through the use of a double-layer structure consisting of an over- and under-layer. It is well documented that the efficiency of a TiO₂ DSSC for light scattering is strongly dependent on refractive index, grain size and size distribution of the TiO₂ particles [18]. The rutile crystalline form of TiO₂ has higher intrinsic scattering efficiency than the anatase crystal because of its higher refractive index (2.74 vs. 2.56) [19]. However, anatase phase is more favor for photovoltaic application. An over-layer consisting of rutile particles with dimensions of 300–400 nm has been widely employed in a traditional DSSC to scatter the incident light [20]. Moreover, TiO₂ nanotubes [21], nanowires [22] and large particles [23] as the light scattering layer have been proposed. An alternative approach which is mixing of small and large particles has also been reported [24]. Kim et al. [25] reported that the cell efficiency of a monolayer TiO₂ solar cell made of TiO₂ nanoparticles (i.e., 7.1 %) was improved using a light scattering layer in the form of a double-layer solar cell made of pure TiO₂ nanoparticles as the under-layer and 3 at.% Cr-doped TiO₂ nanoparticles as the over-layer with power conversion efficiency of 8.4 %.

So far, no significant work has been reported on design of a double-layer DSSC composed of Cr-doped TiO₂ films in the forms of under- and over-layers, as transparent and light scattering layers, respectively. In the present work, we have focused on synthesis of Cr-doped TiO₂ nanoparticles with various atomic ratios and phase compositions by a particulate sol–gel method for solar cell application.

Furthermore, the effect of Cr introduction was studied on phase composition, morphology, optical properties and photovoltaic performance of fabricated TiO₂ cells. The optimum atomic ratio of the dopant was obtained for solar cell application and its effect on light scattering layer was compared with that of pure TiO₂.

2 Experimental

2.1 Preparation of Cr-doped TiO₂ sols and powders

Firstly, TiO₂ sol was prepared according to the method reported in our previous work [26]. Titanium tetraisopropoxide (TTIP) with a purity of 97 % (Aldrich, UK) was used as a titanium precursor; analytical grade hydrochloric acid (HCl) 37 % (Fisher, UK) was used as a catalyst for the peptisation and deionised water was used as a dispersing media. The water–acid mixture (in the range of pH = 1–2) was stabilized at a constant temperature. TTIP was added, forming a white thick precipitate, which gradually peptised after 2 h to form a clear sol. The TiO₂ sol with the concentration of 0.4 M was prepared with TTIP:HCl:H₂O molar ratio of 1:0.5:351.

For preparation of Cr-doped TiO₂ sols CrCl₃·6H₂O (Fluka, UK) was dissolved in TiO₂ sol with different Cr atomic percentages in the range 0–5 at.%. Cr ions can be incorporated into the TiO₂ lattice via displacing Ti⁴⁺ sites due to the close ionic radius of Ti⁴⁺ (60.5 pm) and Cr³⁺ (61.5 pm), forming a Cr-doped TiO₂ [27]. The sols were then heated at 50 °C for 24 h to obtain as-synthesized Cr-doped TiO₂ powders. Subsequently, the as-synthesized powders were annealed at 400 °C for 1 h in air atmosphere to achieve the crystalline powders.

In addition, four different TiO₂ powders, with rutile structure, were prepared for fabrication of the over-layer of the electrode by annealing the following powders at 800 °C for 1 h in air atmosphere: (1) undoped TiO₂ nanopowders, (2) 3 at.% Cr-doped TiO₂ nanopowders, (3) a mixture of 20 wt% commercial TiO₂ powder (99.9 %, Alfa Aesar, USA) and 80 wt% undoped as-synthesized TiO₂ nanopowder and (4) a mixture of 20 wt% commercial TiO₂ powder and 80 wt% Cr-doped TiO₂ as-synthesized nanopowder (with 3 at.% Cr).

2.2 Preparation of DSSCs

2.2.1 Preparation of photoanode electrodes

Basically, two categories of DSSCs, in the forms of mono- and double-layer films, were fabricated in order to study the effect of the dopant concentration and arrangement modes of the double layer films on their photovoltaic

performance. A new formulation of TiO₂ paste was developed in our lab. Both categories of TiO₂ pastes were prepared by mixing the powders, the solvent, the dispersing agents and binders according to the procedure reported in our previous work [28].

The first category, in the form of a monolayer films, were consisted of four different electrodes with various atomic percentages of the dopant (i.e., 0–5 at.%). Four monolayer films were coated on FTO (7 Ω/sq) substrate by spin coating technique from the prepared pastes, as listed in Table 1. The optimal Cr atomic ratio was determined by photovoltaic characteristics of monolayer DSSCs. The second category, in the form of double layer films, were consisted of four different electrodes with the same under-layer (i.e., CT3, which showed the highest efficiency in the first category) and various over-layers (i.e., light scattering layers) with rutile crystalline form, as shown in Table 2.

The deposited films, as photoanode electrodes, were annealed at 400 °C for 2 h in air atmosphere. The post-treatment with TiCl₄ solution was applied to freshly annealed TiO₂ photoanode electrodes as reported in the literature [29]. An aqueous stock solution of 2 M TiCl₄ was diluted to 0.04 M. TiO₂ photoanode electrodes were immersed into this solution and stored in an oven at 70 °C for 30 min in a closed vessel. After flushing with distilled water, the photoanode electrodes were sintered again at 450 °C for 30 min. The resulting electrodes were soaked in 0.3 mM ruthenium (II) dye (Ruthenium 535-bisTBA dye, or N719, Solaronix) solution (using ethanol as a solvent) for 18 h. The photoanode electrodes were washed with ethanol, dried, and then immediately used for photovoltaic measurements.

2.2.2 Preparation of counter electrode

The counter Pt-electrode was deposited on the FTO glass by coating with a drop of H₂PtCl₆ solution (2 mg Pt in 1 ml ethanol) with repetition of the heat treatment at 400 °C for 30 min.

2.2.3 Preparation of electrolyte

The electrolyte employed was a solution of 0.60 M tetrabutyl ammonium iodide, 0.03 M I₂, 0.10 M lithium iodide,

0.10 M guanidinium thiocyanate and 0.50 M 4-tertbutylpyridine in a mixture of acetonitrile and valeronitrile (volume ratio, 85:15).

2.2.4 DSSCs assemblage

The Platinum electrode was placed over the dye-adsorbed photoanode electrodes, and the edges of the cells were sealed with sealing sheet (SX 1170-60, Solaronix). Sealing was accomplished by hot-pressing the two electrodes together at 120 °C. The redox electrolyte was injected into the cells through the small holes and sealed with a small square of sealing sheet. The cell size was 0.25 cm² which corresponds to that of the working electrode.

2.3 Characterisation and measurements

The photoanode electrodes were characterized by X-ray diffraction diffractometer (XRD) using a Philips X'pert PW3020, Cu-K_α and field emission scanning electron microscope (FE-SEM) using a JEOL 6340. The as-synthesized powder was also characterized in thermal behaviour using simultaneous differential thermal (SDT) analysis TASDTQ600, with a heating rate of 5 °C/min in air up to 1,000 °C. The thickness of the electrodes was measured with a Tensor Alpha-step Profiler. The absorption spectrum was analyzed by Ultraviolet–visible (UV–vis) spectroscopy using a 6705 JENWAY spectrometer. The diffuse reflectance spectroscopy (DRS) measurements of the films were recorded using an AVASPEC-2048-TEC spectrometer. The density of the nanostructures was measured by a Micromeritics AccuPyc 1330 pycnometer analyzer. Photovoltaic measurements of fabricated solar cells were carried out using a solar simulator under standard test conditions (STC i.e., irradiance of 100 mW/cm², AM 1.5 spectrum).

3 Results and discussion

3.1 Thermal analysis

Simultaneous differential thermal analysis of 3 at.% Cr-doped TiO₂ powder is shown in Fig. 1. It is evident that the powder undergoes endothermic dehydration in the temperature range 20–126 °C, which is supported by the corresponding weight loss in the TGA curve. The exothermic peaks corresponding to anatase crystallization and the anatase to rutile phase transformation are not observed due to the gradual formation of these phases. The TGA curve shows that the weight loss occurs at two stages, namely, below 126 °C and between 126 and 400 °C. In the first region (below 126 °C), the weight loss of 12.1 % is due to the evaporation of physically adsorbed water from pores. In

Table 1 Characteristics of fabricated monolayer DSSCs

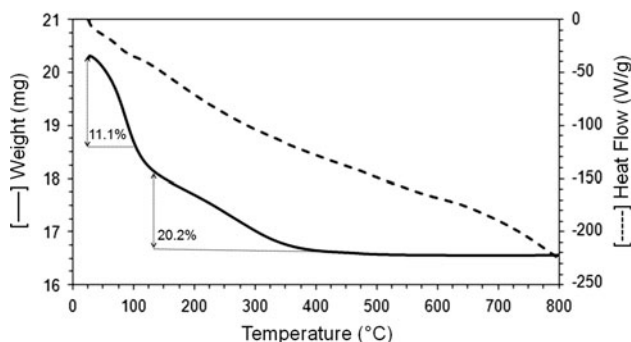
Electrode	Cr at. %	Morphology	Crystal structures
CT0	0	Nanoparticles	A + R
CT1	1	Nanoparticles	A + R + B
CT3	3	Nanoparticles	A + R + B
CT5	5	Nanoparticles	A + R + B

A anatase, R rutile, B brookite

Table 2 Characteristics of fabricated double layer DSSCs

Electrode	Under-layer			Over-layer		
	Cr at. %	Morphology	Crystal structures	Cr at. %	Morphology	Crystal structures
CT3/N0	3	Nanoparticles	A + R + B	0	Nanoparticles	R
CT3/N3	3	Nanoparticles	A + R + B	3	Nanoparticles	R
CT3/NM0	3	Nanoparticles	A + R + B	0	Nanoparticles + microparticles	R
CT3/NM3	3	Nanoparticle	A + R + B	3	Nanoparticles + microparticles	R

A anatase, R rutile, B brookite

**Fig. 1** SDT curve of 3 at.% Cr-doped TiO₂ powder

the second stage (in the range 126–400 °C), the weight loss of 20.2 % is due to dehydroxylation and removal of residual organics. There is no weight loss at temperatures above 400 °C. Consequently, the ultimate annealing temperature for entire elimination of organic and inorganic components is determined at 400 °C.

3.2 Crystal structure

The crystal structure and phase composition of deposited transparent films were studied by XRD analysis and the results were shown in Fig. 2. It can be observed that, CT0 film had a mixture of anatase and rutile phases by dominant peaks at $2\theta = 25.3^\circ$ (1 0 1), and $2\theta = 27.5^\circ$ (1 1 0), respectively, whereas other transparent films showed a mixture of anatase, rutile and brookite phases by dominant peaks at $2\theta = 25.3^\circ$ (1 0 1), $2\theta = 27.5^\circ$ (1 1 0), and $2\theta = 25.3^\circ$ (1 2 0), respectively. Therefore, introduction of Cr into TiO₂ lattice led to formation of brookite phase. The heat treatment of Cr-doped TiO₂ films at 400 °C resulted in anatase to brookite phase transformation rather than anatase to rutile transformation. This can be related to reduction of anatase crystallite size by introducing Cr into TiO₂. The anatase to rutile phase transformation is known to be a nucleation and growth process during which rutile nuclei form within the anatase phase and grow in size. Crystallites should grow to the critical nuclei size before the transformation can proceed. Consequently, formation of rutile

nuclei retards by Cr introduction since the initial crystallites have the smaller size than the critical nuclei size. Moreover, over the time scales accessible to molecular dynamics simulations has been reported that annealing of anatase and amorphous nanoparticles results in a brookite agglomerate whereas the final annealed agglomerate transforms to the rutile phase [30]. It has been reported that brookite-TiO₂ phase exhibits higher photocatalytic activity than rutile and anatase structures and, therefore, brookite can be a good candidate for photovoltaic devices [31, 32]. Consequently, the presence of brookite within the Cr-doped TiO₂ films could improve the photovoltaic performance of the cells. Moreover, neither chromium oxide nor chromium titanates were detected for Cr-doped TiO₂ films due to low concentration of the dopant. It can be observed that, the phase composition of Cr-doped TiO₂ films depends on dopant concentration. The mass fraction of anatase (W_A), rutile (W_R) and brookite (W_B) in the crystal lattice can be calculated based on the relationship among the integrated intensities of anatase (1 0 1), rutile (1 1 0) and brookite (1 2 1) peaks by the following formula, developed by Zhang and Banfield [33] and Gribb and Banfield [34].

$$W_A = \frac{0.886A_a}{0.886A_a + A_r + 2.721A_b} \quad (1)$$

$$W_R = \frac{A_r}{0.886A_a + A_r + 2.721A_b} \quad (2)$$

$$W_B = \frac{2.721A_b}{0.886A_a + A_r + 2.721A_b} \quad (3)$$

where A_a , A_r and A_b are the integrated peak intensities of the anatase (1 0 1), rutile (1 1 0) and brookite (1 2 1) peaks, respectively. Moreover, the average crystallite size of crystalline anatase, rutile and brookite phases was calculated by the Scherrer equation as follows [35]:

$$d = \frac{k\lambda}{B \cos \theta} \quad (4)$$

where d is the crystallite size, k is a constant of 0.9, λ is the X-ray wavelength of Cu which is 1.5406 Å, θ is the Bragg angle in degree, and B is the full width at half maximum (FWHM) of the peak.

Fig. 2 XRD patterns of the under-layer of photoanode electrodes annealed at 400 °C: *a* CT0, *b* CT1, *c* CT3 and *d* CT5. *A* anatase-TiO₂, *R* rutile-TiO₂, *B* brookite-TiO₂

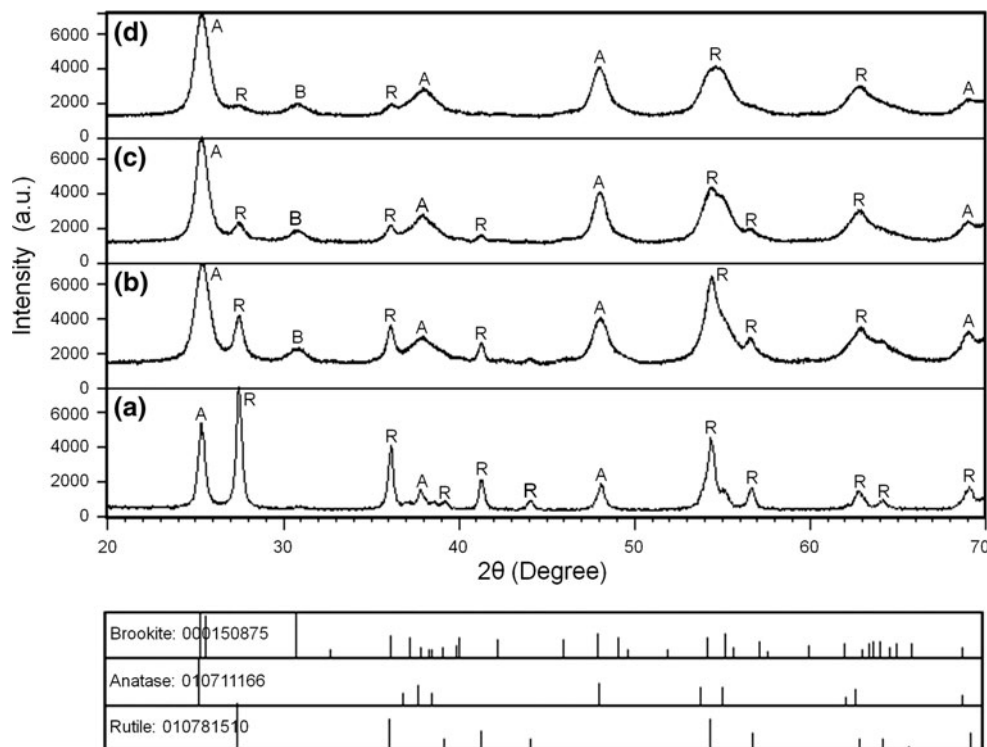


Table 3 The phase composition and crystallite size of the under- and over-layer of deposited photoanode electrodes

Film	Phase composition (%)			Crystallite size (nm)			
	Anatase	Rutile	Brookite	Anatase	Rutile	Brookite	Average
CT0	36	64	0	20.6	38.2	–	29.4
CT1	54	27	19	07.4	25.0	03.8	12.1
CT3	70	11	19	08.5	21.7	04.3	11.5
CT5	78	3	19	07.1	17.9	04.6	09.9
CT3/N0	0	100	0	–	47.0	–	47.0
CT3/N3	0	100	0	–	41.2	–	41.2
CT3/NM0	0	100	0	–	48.0	–	48.0
CT3/NM3	0	100	0	–	43.5	–	43.5

The mass fraction of anatase, rutile and brookite phases as well as their average crystallite size is shown in Table 3. It is evident that the anatase content of the under-layer films was increased with increasing dopant concentration, whereas their brookite content was independent of Cr concentration. Furthermore, the crystal growth of TiO₂ films was hindered by Cr introduction, resulting in reducing the average crystallite size of the films. These results are in good agreement with those reported by Ruiz et al. [36].

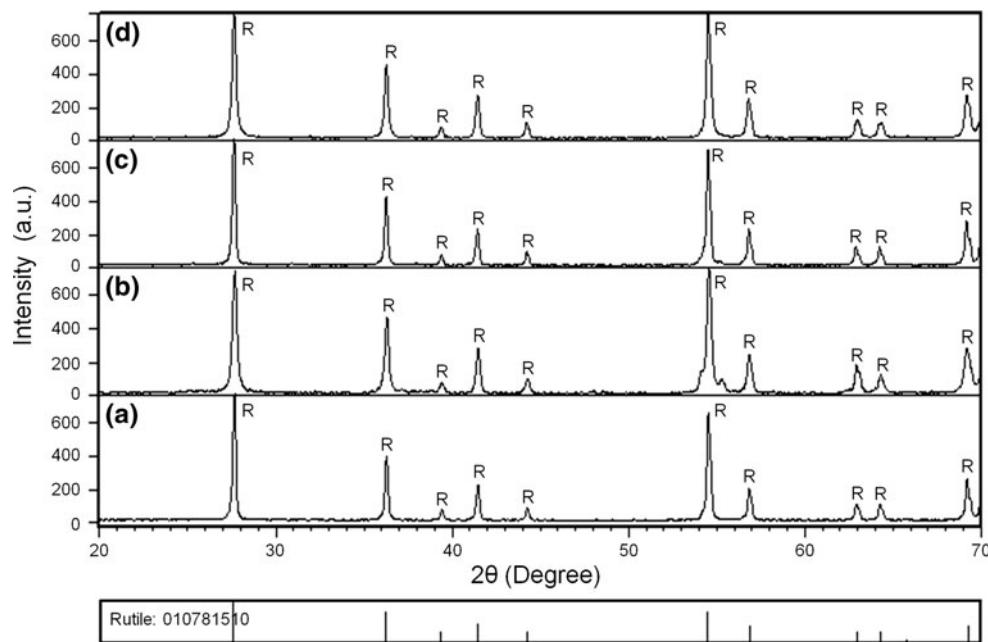
Figure 3 shows XRD patterns of the over-layer of photoanode electrodes annealed at 800 °C. It is evident that, all films showed highly pure crystalline rutile phase by the dominant peak at $2\theta = 27.5^\circ$ (1 1 0). Both undoped

and Cr-doped TiO₂ electrodes showed rutile structure at high annealing temperature of 800 °C. Therefore, the anatase to rutile phase transformation is more dependent on annealing temperature than doping with desired element. It can be seen that, the crystallite size of rutile phase was decreased with introduction of 3 at.% Cr into TiO₂ lattice. As expected, the rutile crystallite size of electrodes composed of mixtures of nanoparticles and microparticles is higher than those made of pure nanoparticles.

3.3 Microstructure

Figure 4 shows surface morphology of deposited under-layer films. It is evident that, all deposited films had almost

Fig. 3 XRD patterns of the over-layer of photoanode electrodes annealed at 800 °C: *a* CT3/N0, *b* CT3/N3, *c* CT3/NM0 and *d* CT3/NM3. *R* rutile-TiO₂



uniform, homogeneous and porous structure as a result of removal of the dispersing agent and solvents. As can be observed, the porosity of doped electrodes was higher than that of undoped electrode, enhancing dye adsorption. This can be explained by the fact that the decomposition of chromium chloride hexahydrate is an exothermic reaction and the released heat avoids sintering the particles, resulting in increasing the porosity. Moreover, the porosity of doped films depended on the dopant concentration. It was decreased with increasing Cr atomic percentage up to 5 at.%. Porosity is an essential parameter for a high-efficiency DSSC, because it allows adsorption of sufficiently large number of dye molecules needed for efficient light harvesting, as confirmed by a spectroscopic method (see Sect. 3.5.1). On the other hand, large pores may act as electron traps, resulting in reduction of cell efficiency. This can be related to the depth of traps that participate in the electron motion which affect the value of the diffusion coefficient [37]. Therefore, an optimum porosity of photoanode electrode enhances the photovoltaic performance of a DSSC.

Figure 5 illustrates cross sectional view and surface image of double layer CT3/NM3 photoanode electrode annealed at 400 °C. The thickness of the film can be controlled by spin coating parameters. These parameters were tailored to obtain a total thickness of 14 μm. It can be observed that the under- and over-layer had almost the same thickness around 7 μm. The surface image showed a mixture of micro- and nano-particles due to addition of commercial TiO₂ powder with micron size particles into the synthesized 3 at.% Cr-doped TiO₂ nanoparticles. Incorporation of large particles with nanoparticles led to

improvement of the light-scattering effect of the double layer electrode (see Sect. 3.5.2).

3.4 UV–vis analysis

Optical absorbance spectra of the doped and undoped TiO₂ nanoparticles are shown in Fig. 6. It can be seen that the UV–vis absorbance of Cr-doped TiO₂ significantly shifts to longer wavelength (i.e., red shift) in comparison with that of the pure TiO₂ due to acceptor nature of Cr within TiO₂ structure. Consequently, Cr introduction may enhance the visible light absorption property of the material by shifting the absorption onset to visible region, thus utilizing the maximum portion of solar light.

To quantify the optical band gap of the nanoparticles, Tauc Model [38] was employed in the high absorbance region of the transmittance spectra according to the following equation:

$$\alpha hv = A(hv - E_g)^r \quad (5)$$

where hv is the photon energy, E_g is the optical band gap, A is a constant which does not depend on photon energy, r has four numeric values (1/2 for allowed direct, 2 for allowed indirect, 3 for forbidden direct and 3/2 for forbidden indirect optical transitions) and α is the absorption coefficient which is calculated from the following equation:

$$\alpha = \frac{2.303K \cdot \rho}{L \cdot C} \quad (6)$$

where K is the absorbance of the sample; ρ is the density of TiO₂ nanoparticles; C is the concentration of the nanoparticles and L is the optical path length. The density of

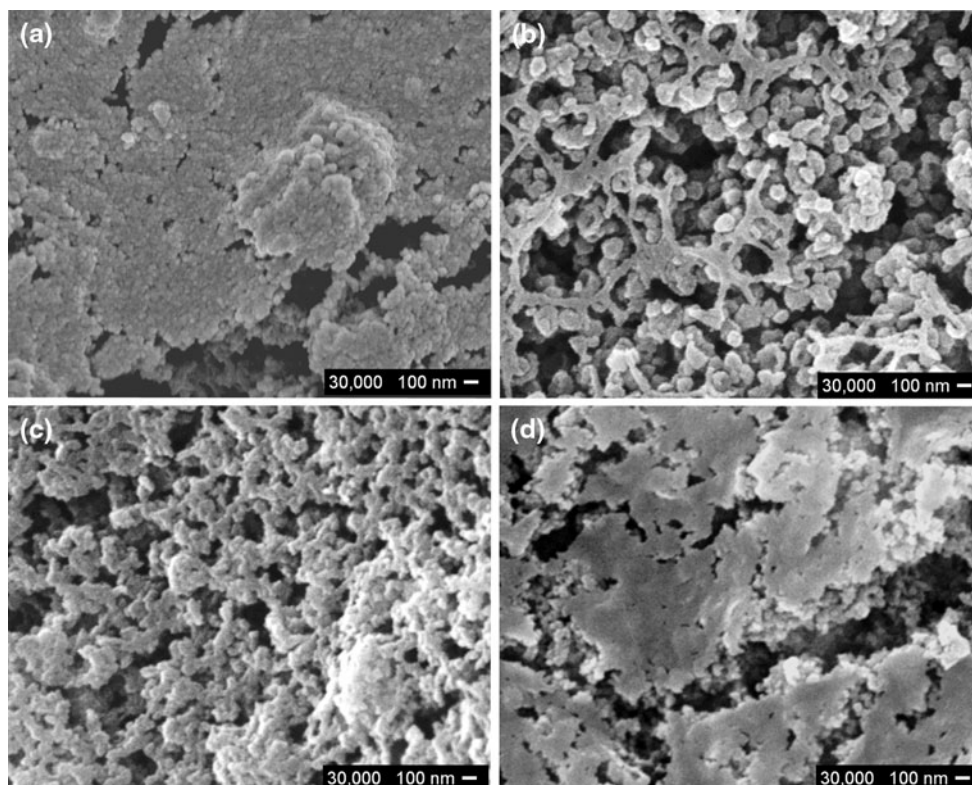


Fig. 4 FE-SEM images of surface morphology of 400 °C annealed monolayer TiO₂ electrodes doped with different Cr atomic percentages: **a** CT0, **b** CT1, **c** CT3 and **d** CT5

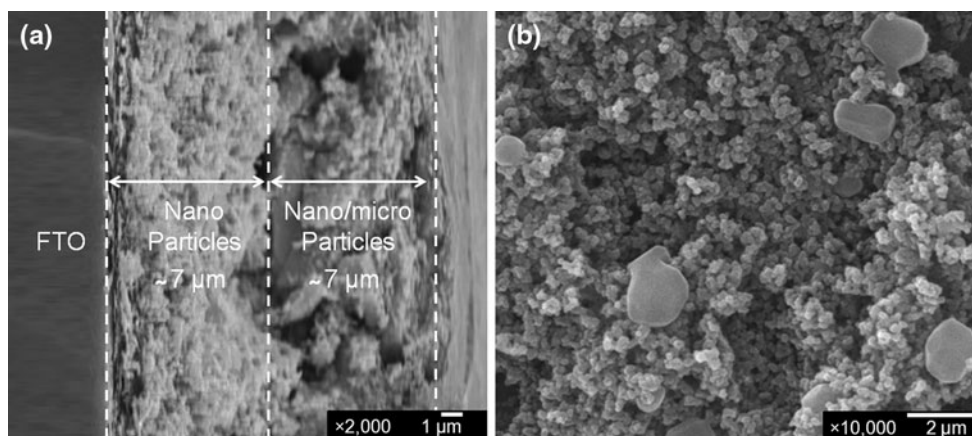


Fig. 5 FE-SEM images of double layer CT3/NM3 electrode annealed at 400 °C: **a** cross sectional view and **b** surface morphology

CT0, CT1, CT3 and CT5 nanopowders was measured 4.16, 4.04, 3.97 and 3.89 g/cm³, respectively. The indirect band gap of nanoparticles was determined by plotting $(\alpha h\nu)^{0.5}$ versus $h\nu$, with the extrapolation of the linear region to the low energies, being 3.17, 2.99, 2.74 and 2.65 eV for CT0, CT1, CT3 and CT5 films, respectively. It is evident that the optical band gap energy of the films was decreased with increasing dopant concentration. Due to the lower band gap energy of doped nanoparticles, it is expected their light

absorption and light scattering are greater than those of undoped particles.

3.5 Photovoltaic performance of DSSCs

3.5.1 Effect of Cr atomic percentage of monolayer DSSCs

The photocurrent density–voltage (J–V) characteristics of fabricated monolayer TiO₂ DSSCs, with the same

Fig. 6 Optical absorbance spectra and the plots of $(\alpha h\nu)^{0.5}$ versus photon energy of monolayer TiO₂ photoanode electrodes doped with different Cr atomic percentages: **a** CT0, **b** CT1, **c** CT3 and **d** CT5

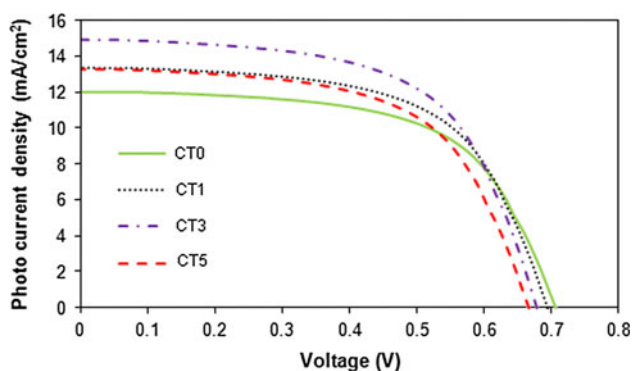
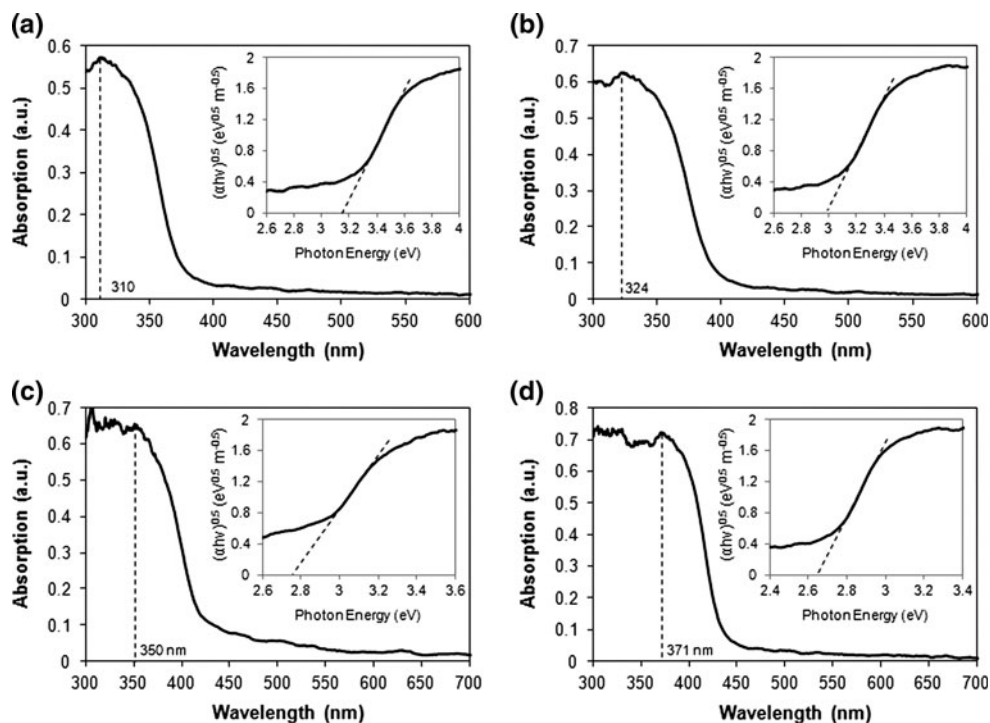


Fig. 7 Photocurrent density–voltage curve of monolayer TiO₂ DSSCs doped with different Cr concentrations

thickness (i.e., 14 μm), were illustrated in Fig. 7. In addition, the corresponding photovoltaic parameters such as short circuit current (J_{SC}), open circuit voltage (V_{OC}), fill factor (FF), adsorbed dye and power conversion efficiency (η) were summarized in Table 4. As can be observed, the solar cells made of doped TiO₂ nanoparticles had smaller V_{OC} than that of made of undoped TiO₂, as a result of smaller energy difference between the conduction band of nanoparticles and the iodine redox potential [39]. It is evident that the short circuit current and power conversion efficiency of the solar cells changed with Cr atomic percentage, reaching a maximum at a specific value. Therefore, CT3 solar cell showed the highest power conversion efficiency of 6.10 % amongst all fabricated solar cells. The

Table 4 Photovoltaic parameters of fabricated monolayer TiO₂ DSSCs doped with different Cr atomic percentages

DSSC	V_{OC} (mV)	J_{SC} (mA/cm ²)	FF (%)	η (%)	Adsorbed dye (10 ⁸ mol/cm ²)
CT0	706	11.98	61.11	5.18	8.74
CT1	695	13.35	60.83	5.65	9.12
CT3	678	14.87	60.39	6.10	9.68
CT5	666	13.29	60.02	5.32	8.31

improvement in the photovoltaic performance of CT3 cell can be explained due to enhancement of J_{SC} by the following mechanisms.

Firstly, introduction of Cr into TiO₂ lattice can improve its photo-response by introducing additional energy levels within the band gap of TiO₂. Chromium dopant modifies the electronic structure of TiO₂ and forms localized acceptor levels in the forbidden band gap. This modifies the concentration of electrons and electron holes and leads to a decrease in the internal electrical resistances [15]. Secondly, the appropriate morphology of CT3 film due to an optimum porosity causes considerable improvement in surface area and, therefore, enhancing dye adsorption. The amount of adsorbed dye was determined by a spectroscopic method by measuring the concentration of desorbed dye on the titania surface into solution of 0.1 molar NaOH [40]. The absorbance of N719 dye on the CT3 electrode was found to be greater than the rest of the electrodes at the dye spectral maximum (308 nm), as shown in Fig. 8. Thirdly, it

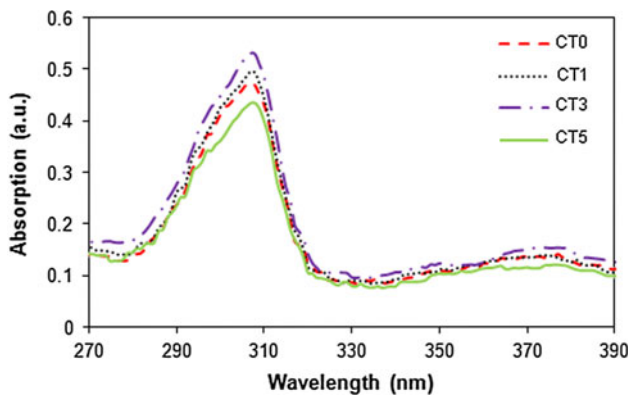


Fig. 8 Optical absorbance spectra of N719-coated monolayer TiO₂ photoanode electrodes doped with different Cr atomic percentages

has been reported that TiO₂ DSSC prepared with a mixture of anatase and rutile with weight ratio of 9:1 shows the most prominent performance in comparison with those prepared with other phase compositions due to the electron-holes separation at the interface between phases [41–46]. As shown in Table 3, CT3 cell had almost the same anatase to rutile weight ratio of 9:1 and, therefore, the synergistic effect between anatase and rutile significantly improves the photovoltaic activity of anatase.

3.5.2 Effect of light scattering layer of double layer DSSCs

As mentioned in introduction section, the rutile crystalline form of TiO₂ has higher refractive index than anatase and, therefore, deposition of an over-layer with rutile structure could improve light scattering and short current density of the DSSCs. To study such phenomenon, four double-layer DSSCs with the same under-layer film (i.e., CT3 film) and different light scattering over-layers were fabricated and compared with those of monolayer DSSCs. The photocurrent density–voltage (J–V) characteristics of fabricated double-layer DSSCs were illustrated in Fig. 9. In addition, the corresponding photovoltaic parameters were summarized in Table 5. It is evident that, CT3/NM3 solar cell had the highest short circuit current and power conversion efficiency of 17.32 mA/cm² and 7.02 %, respectively amongst all fabricated monolayer and double-layer solar cells. The most likely reason for enhancement of the cell efficiency can be explained by the following mechanisms.

Firstly, CT3 film was used as the under-layer which had the highest photovoltaic performance amongst all monolayer DSSC. Secondly, the presence of rutile in the over-layer limited electron transport due to its constraints. On one hand, the internal resistance of rutile phase is higher than that of anatase phase due to 90° rotated octahedral connected by their edges in the case of rutile compared to arrangement of parallel octahedral connected by their vertices in the case of anatase. On the other hand, lower

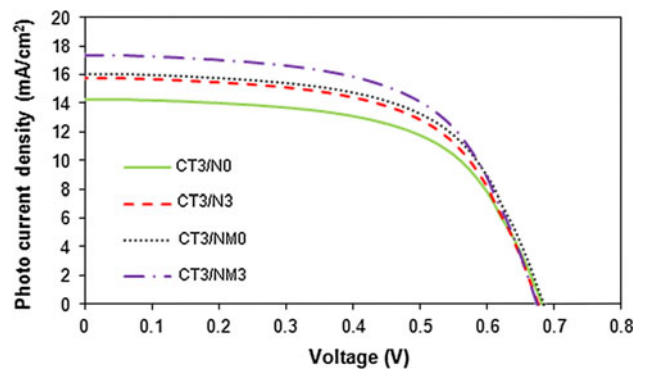


Fig. 9 Photocurrent density–voltage curves of double-layer TiO₂ DSSCs doped with different Cr percentages

Table 5 Photovoltaic parameters of double-layer DSSCs with different light scattering layers

DSSC	V _{oc} (mV)	J _{sc} (mA/cm ²)	FF (%)	η (%)	Adsorbed dye (10 ⁸ mol/cm ²)
CT3/N0	682	14.27	60.45	5.86	07.83
CT3/N3	677	15.70	60.31	6.42	08.11
CT3/NM0	684	16.03	60.51	6.64	07.74
CT3/NM3	674	17.32	60.27	7.02	07.95

surface area of rutile nanoparticles (i.e., 49 m²/g), in comparison to that of anatase nanoparticles (i.e., 117 m²/g), constrains dye sensitization and correspondingly short circuit current. Consequently, Cr introduction in the over-layer, as well as under-layer, is one promising solution to this impasse by inducing electron transport rate due to reduction of rutile crystallite size as well as the optical band gap energy. Thirdly, the deposited over-layer induced improvement of light scattering by multiple scattering of photons, resulting in an increase in optical path length. Although deposition of the light scattering layer containing mixtures of micro- and nano-particles induced a considerable decline in the amount of adsorbed dye in the double-layer cells, the effect of light scattering which led to rising light-harvesting of the cell was dominant, resulting in enhancement of J_{sc}. This was studied by evaluating the light scattering property of the dye-free over-layers (i.e., N0, N3, NM0 and NM3 films) by DRS. The CT0 film was used as a reference and the light scattering property of other films was studied. The diffuse reflectance spectra of the over-layers are shown in Fig. 10. In all measurements, the samples were irradiated from the side of the glass substrate on which the film was not deposited. When a beam of solar light passes the FTO glass and contacts with the films, the incident light is supposed to be reflected, scattered and transmitted within the films. In general, the part of incident light scattered within a film and returned to the surface is considered to be diffused reflectance [47].

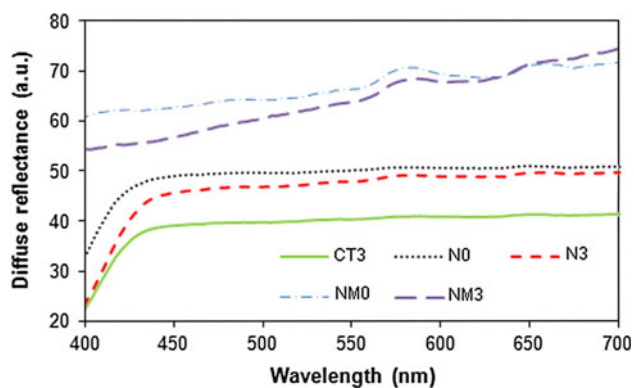


Fig. 10 Diffuse reflectance spectra of light scattering layers in double layer DSSCs

The layers containing nano- and micro-particles (i.e., NM0 and NM3 layers) exhibited higher light scattering property than those composed of nanoparticles (i.e., N0 and N3), as can be inferred from the higher diffuse reflectance of these samples at higher wavelengths (where TiO_2 does not absorb). It can be seen that, Cr-doped layers showed lower light scattering property than undoped layers due to smaller rutile crystallite size, as mentioned in Sect. 3.2. Consequently, a systematic design of double-layer cells by tailoring their phase composition, morphology, electron transport and light scattering of the over-layer can improve the photovoltaic performance of Cr-doped TiO_2 dye sensitized solar cells.

4 Conclusions

Two effective methods were presented in order to make a balance among electron injection, light scattering effect and dye absorption of photoanode electrode of dye-sensitized solar cells. For this purpose, a systematic study of the DSSCs by fabrication of monolayer Cr-doped TiO_2 films with different atomic percentages (i.e., 0–5 at.%) and double layer films with various rutile light scattering layers with different morphologies and phase compositions was performed.

XRD and SEM analyses revealed that, Cr introduction hindered anatase to rutile phase transformation as well as grain growth during annealing process. UV–vis analysis showed that the absorbance of Cr-doped TiO_2 significantly shifted to longer wavelength (the red shift) in comparison with that of the pure TiO_2 . The Cr-doped films showed higher light absorption and scattering due to the lower optical band gap energy. Photoanode electrode containing 3 at.% Cr (i.e., CT3 solar cell) showed the maximum power conversion efficiency of 5.92 % among monolayer DSSCs due to synergistic effect between anatase and rutile as well as a decrease in the internal electrical resistances as

a result of Cr introduction into TiO_2 lattice. The double-layer DSSC made of CT3 film as the under-layer and mixtures of Cr-doped TiO_2 nanoparticles and microparticles with rutile phase, as the over-layer (i.e., CT3/NM3 solar cell) showed the highest power conversion efficiency of 7.02 % among all fabricated cells. The improved photoelectrical performance of CT3/NM3 solar cell was attributed to high light scattering due to presence of microparticles in the over-layer, as confirmed by DRS. Moreover, this cell had high electron injection due to decrease in optical band gap energy of both under- and over-layers, as a result of doping with Cr.

Acknowledgments The authors would like to thank Iran Nanotechnology Initiative Council for the financial support.

References

- O'Regan B, Grätzel M (1991) A low-cost, high-efficiency solar cell based on dye-sensitized colloidal TiO_2 films. *Nature* 353:737–739
- Yella A, Lee HW, Tsao HN, Yi C, Chandiran AK, Nazeeruddin MK, Diau EWG, Yeh CY, Zakeeruddin SM, Grätzel M (2011) Protoporphyrin-sensitized solar cells with cobalt (II-III)-based redox electrolyte exceeds 12 percent efficiency. *Science* 334:629–634
- Hagfeldt A, Grätzel M (2000) Molecular photovoltaics. *Acc Chem Res* 33:269–277
- Fujishima A, Zhang X, Tryk DA (2008) TiO_2 photocatalysis and related surface phenomena. *Surf Sci Rep* 63:515–582
- Su R, Bechstein R, Kibsgaard J, Vang RT, Besenbacher F (2012) High-quality Fe-doped TiO_2 films with superior visible-light performance. *J Mater Chem* 22:23755–23758
- Kim DH, Lee KS, Kim YS, Chung YC, Kim SJ (2006) Photocatalytic activity of Ni 8 wt%-doped TiO_2 photocatalyst synthesized by mechanical alloying under visible light. *J Am Ceram Soc* 89:515–518
- Karunakaran C, Abiramasundari G, Gomathisankar P, Manikandan G, Anandi V (2010) Cu-doped TiO_2 nanoparticles for photocatalytic disinfection of bacteria under visible light. *J Colloid Interface Sci* 352:68–74
- Deng GR, Xia XH, Guo ML, Gao Y, Shao G (2011) Mn-doped TiO_2 nanopowders with remarkable visible light photocatalytic activity. *Mater Lett* 65:2051–2054
- Matsumoto Y, Murakami M, Shono T, Hasegawa T, Fukumura T, Kawasaki M, Ahmet P, Chikyow T, Koshihara SY, Koinuma H (2001) Room-temperature ferromagnetism in transparent transition metal-doped titanium dioxide. *Science* 291:854–856
- Lü X, Mou X, Wu J, Zhang D, Zhang L, Huang F, Xu F, Huang S (2010) Improved-performance dye-sensitized solar cells using Nb-doped TiO_2 electrodes: efficient electron injection and transfer. *Adv Funct Mater* 20:509–515
- Choudhury B, Choudhury A (2012) Dopant induced changes in structural and optical properties of Cr^{3+} doped TiO_2 nanoparticles. *Mater Chem Phys* 132:1112–1118
- Yu JC, Li GS, Wang XC, Hu XL, Leung CW, Zhang ZD (2006) An ordered cubic $\text{Im}\bar{3}m$ mesoporous Cr– TiO_2 visible light photocatalyst. *Chem Commun* 25:2717–2719
- Irie H, Shibamura T, Kamiya K, Miura S, Yokoyama T, Hashimoto K (2010) Characterization of Cr(III)-grafted TiO_2 for photocatalytic reaction under visible light. *Appl Catal B Environ* 96:142–147

14. Peng YH, Huang GF, Huang WQ (2012) Visible-light absorption and photocatalytic activity of Cr-doped TiO₂ nanocrystal films. *Adv Powder Technol* 23:8–12
15. Lyson B, Gwizdz P, Czapl A, Lubecka M, Zakrzewska K, Biernacka K, Radecka M, Michalow-Mauke M, Graule T, Balogh AG, Lauterbach S, Kleebe HG (2011) TiO₂:Cr nanopowders for hydrogen sensing. *Procedia Eng* 25:749–752
16. Xie Y, Huang N, You S, Liu Y, Sebo B, Liang L, Fang X, Liu W, Guo S, Zhao XZ (2013) Improved performance of dye-sensitized solar cells by trace amount Cr-doped TiO₂ photoelectrodes. *J Power Sources* 224:168–173
17. Zhang Q, Cao G (2011) Nanostructured photoelectrodes for dye-sensitized solar cells. *Nano Today* 6:91–109
18. Johnson RW, Thiele ES, French RH (1997) Light-scattering efficiency of white pigments: an analysis of model core-shell pigments vs. optimized rutile TiO₂. *Tappi J* 80:233–239
19. Ross WD (1971) Theoretical computation of light scattering power: comparison between TiO₂ and air bubbles. *J Paint Technol* 43:50–66
20. Hore S, Vetter C, Kern R, Smit H, Hinsch A (2006) Influence of scattering layers on efficiency of dye-sensitized solar cells. *Sol Energ Mater Sol C* 90:1176–1188
21. Xu H, Tao X, Wang DT, Zheng YZ, Chen JF (2010) Enhanced efficiency in dye-sensitized solar cells based on TiO₂ nanocrystal/nanotube double-layered films. *Electrochim Acta* 55:2280–2285
22. Bakhshayesh AM, Mohammadi MR, Fray DJ (2012) Controlling electron transport rate and recombination process of TiO₂ dye-sensitized solar cells by design of double-layer films with different arrangement modes. *Electrochim Acta* 78:384–391
23. Kong FT, Dai SY, Wang KJ (2007) Review of recent progress in dye-sensitized solar cells. *Adv Optoelectron* 2007:1–13
24. Yanagida M, Onozawa-Komatsuzaki N, Kurashige M, Sayama K, Sugihara H (2010) Optimization of tandem-structured dye-sensitized solar cell. *Sol Energ Mat Sol C* 94:297–302
25. Kim C, Kim KS, Kim HY, Han YS (2008) Modification of a TiO₂ photoanode by using Cr-doped TiO₂ with an influence on the photovoltaic efficiency of a dye-sensitized solar cell. *J Mater Chem* 18:5809–5814
26. Mohammadi MR, Ghorbani M, Cordero-Cabrera MC, Fray DJ (2006) Synthesis of high surface area nanocrystalline anatase-TiO₂ powders derived from particulate sol-gel route by tailoring processing parameters. *J Sol-Gel Sci Technol* 40:15–23
27. Shannon RD (1976) Revised effective ionic radii and systematic studies of interatomic distances in halides and chalcogenides. *Acta Crystallogr A* 32:751–767
28. Mohammadi MR, Louca RRM, Fray DJ, Welland ME (2012) Dye-sensitized solar cells based on a single layer deposition of TiO₂ from a new formulation paste and their photovoltaic performance. *Sol Energ* 86:2654–2664
29. Ito S, Liska P, Pechy P, Bach U, Nazeeruddin MK, Kay A, Zakeeruddin SM, Grätzel M (2005) Control of dark current in photoelectrochemical (TiO₂/I⁻-I³⁻) and dye-sensitized solar cells. *Chem Commun* 34:4351–4353
30. Koparde VN, Cummings PT (2008) Phase transformations during sintering of titania nanoparticles. *ACS Nano* 2:1620–1624
31. Bakardjieva S, Stengl V, Szatmary L, Subrt J, Lukac J, Murafa N, Niznansky D, Cizek K, Jirkovsky J, Petrova N (2006) Transformation of brookite-type TiO₂ nanocrystals to rutile: correlation between microstructure and photoactivity. *J Mater Chem* 16:1709–1716
32. Yan BF, Chen B, Mahurin SM, Schwartz V, Mullins DR, Lupini AR, Pennycook SJ, Dai S, Overbury SH (2005) Preparation and comparison of supported gold nanocatalysts on anatase, brookite, rutile, and P25 polymorphs of TiO₂ for catalytic oxidation of CO. *J Phys Chem B* 109:10676–10685
33. Zhang H, Banfield JF (2000) Understanding polymorphic phase transformation behavior during growth of nanocrystalline aggregates: insights from TiO₂. *J Phys Chem B* 104:3481–3487
34. Gribb A, Banfield JF (1997) Particle size effects on transformation kinetics and phase stability in nanocrystalline TiO₂. *Am Mineral* 82:717–728
35. Cullity BD (1987) *Elements of X-ray diffraction*. Addison-Wesley Publishing Company, London
36. Ruiz AM, Sakai G, Cornet A, Shimanoe K, Morante JR, Yamazoe N (2003) Cr-doped TiO₂ gas sensor for exhaust NO₂ monitoring. *Sens Actuators B Chem* 93:509–518
37. Grätzel M (2005) Solar energy conversion by dye-sensitized photovoltaic cells. *Inorg Chem* 44:6841–6851
38. Tauc J (1974) *Amorphous and liquid semiconductors*. Plenum Press, London
39. Qi L, Liu Y, Li C (2010) Controlled synthesis of TiO₂-B nanowires and nanoparticles for dye-sensitized solar cells. *Appl Surf Sci* 257:1660–1665
40. Feigenbrugel V, Loew C, Calvé SL, Mirabel P (2005) Near-UV molar absorptivities of acetone, alachlor, metolachlor, diazinon and dichlorvos in aqueous solution. *J Photochem Photobiol A Chem* 174:76–81
41. Chen L, Graham ME, Li G, Gray KA (2006) Fabricating highly active mixed phase TiO₂ photocatalysts by reactive DC magnetron sputter deposition. *Thin Solid Films* 515:1176–1181
42. Li G, Ciston S, Saponjic Z, Chen L, Dimitrijevic N, Rajh T, Gray KA (2008) Synthesizing mixed-phase TiO₂ nanocomposites using a hydrothermal method for photo-oxidation and photoreduction applications. *J Catal* 253:105–110
43. Li G, Chen L, Graham ME, Gray KA (2007) A comparison of mixed phase titania photocatalysts prepared by physical and chemical methods: the importance of the solid-solid interface. *J Mol Catal A Chem* 275:30–35
44. Hurum DC, Agrios AG, Gray KA, Rajh T, Thurnauer MC (2003) Explaining the enhanced photocatalytic activity of Degussa P25 mixed-phase TiO₂ using EPR. *J Phys Chem B* 107:4545–4549
45. Wang H, Su C, Chen HS, Liu YC, Hsu YW, Hsu NM, Li WR (2011) Preparation of nanoporous TiO₂ electrodes for dye-sensitized solar cells. *J Nanomater*. doi:10.1155/2011/547103
46. Kim BM, Rho SG, Kang CH (2011) Effects of TiO₂ structures in dye-sensitized solar cell. *J Nanosci Nanotechnol* 11:1515–1517
47. Yang L, Lin Y, Jia J, Xiao X, Li X, Zhou X (2008) Light harvesting enhancement for dye-sensitized solar cells by novel anode containing cauliflower-like TiO₂ spheres. *J Power Sources* 182:370–376